IJE TRANSACTIONS B: Applications Vol. 37 No. 08, (August 2024) 1475-1485

International Journal of Engineering

Journal Homepage: www.ije.ir

Numerical Investigation of Interceptor Bulb to Improve Trim Control

S. Yulianti, S. Samuel*, P. Manik, S. T. P. Ahmad

Naval Architecture Department, Diponegoro University, Semarang, Central Java, Indonesia

P A P E R I N F O

Paper history:
Received 10 September 2023
Received in revised form 03 January 2024
Accepted 31 January 2024

Keywords:
Bulb Interceptor
Finite Volume Method
Drag
Rectangular Interceptor
Unmanned Surface Vehicle

A B S T R A C T

This study addresses interceptor devices to improve the hydrodynamic characteristic of autonomous unmanned surface vehicle (USV). The bulb and rectangular interceptors had molded on a planning hull. This research aims to mitigate drag impact on rectangular interceptors at high speeds. According to this study, a bulb interceptor had a better impact than a rectangular interceptor. This research is based on the finite volume method (FVM) with dynamic fluid-body interaction (DFBI), which captured the ship's dynamic trim and sinkage. The simulation used an overset mesh technique with two domains as a donor-acceptor cell. Furthermore, numerical calculations using the Reynolds-Averaged Navier-Stokes equation and the k-turbulence model predict the turbulent flow. Grid independence studies and international towing tank conference (ITTC) recommendations have been applied to ensure simulation accuracy. This study reported that the bulb interceptor had effectiveness between 9%-25% compared to the rectangular interceptor at high speed. This research showed that the bulb interceptor had better effectiveness than the rectangular interceptor.

***doi**: 10.5829/ije.2024.37.08b.02*

Graphical Abstract

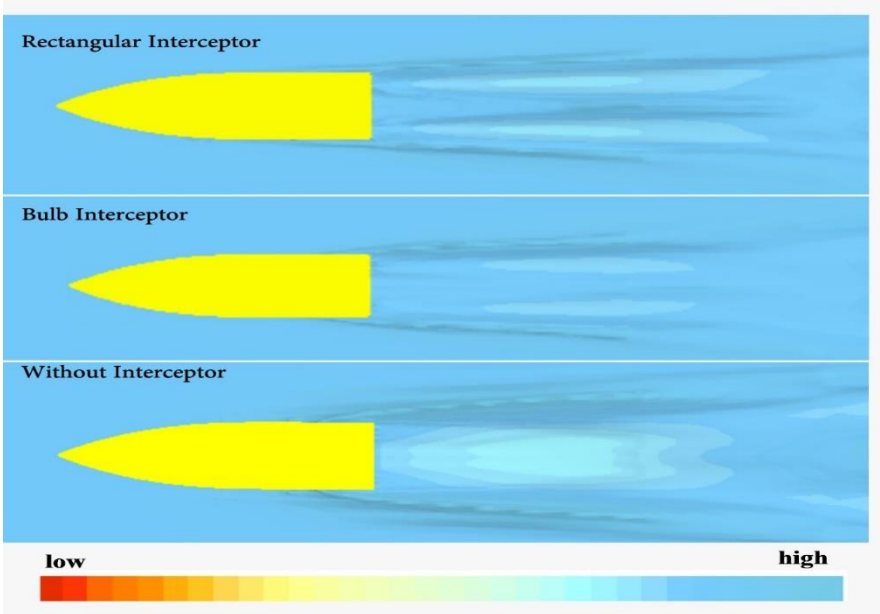

*Corresponding Author Email: samuel@ft.undip.ac.id (S. Samuel)

Please cite this article as: Yulianti S, Samuel S, Manik P, Ahmad STP, Numerical Investigation of Interceptor Bulb to Improve Trim Control. International Journal of Engineering, Transactions B: Applications. 2024;37(08):1475-85.

1. INTRODUCTION

An Unmanned Surface Vehicle (USV) robot automatically operate on the free water surface by providing a reference point. The autonomous unmanned surface vehicle has enamored significant consideration for its advantages in applications to monitoring and patrolling. Many researchers have been undertaking projects to elaborate USV hardware and software algorithms. Conducted research introducing multiple target tracking for the Aragon USV system developed by the Korea Research Institute of Ships and Ocean Engineering (KRISO) (1). Research converse on ship autonomous navigation and avoidance of collusion in maritime traffic circumstances (2). Another paper showed a static obstacle avoidance problem for high-speed USV called Local Reactive Obstacle Avoidance Based on Region Analysis (3). The Aragon-2 is the elaborated USV system involves waterjet propulsion to identify turning characteristics based on an experimental test (4).

Efficiency is a fundamental aspect in designing ships. One of the energy efficiency parameters is the resistance generated during ship operation. Several improvements to reduce ship resistance are to change the shape or modify the hull (5-7). The ship resistance can be decreased by reducing wave or friction resistance using stern flaps (8, 9), hydrofoil (10) and also interceptor-flap hybrid combination (11, 12). Other devices used to improve ship performance are spray deflectors or spray strips. A spray deflector can reduce ship resistance by reducing the wet area of the ship (13). Other research has shown that the spray rail could reduce 2.4% resistance (14), and the spray deflector could reduce 10% to 25% resistance (15). However, modification of the hull or the installation of fixed devices is often difficult to adjust to changes in the speed of the planing phase.

Several research conducted experimental research using an active control device known as an interceptor (16). The interceptor is energy saving device that applied to the stern to control trim. The interceptor is driven by a servomotor and can be adjusted in height in the ship navigation room. The height of the interceptor can be controlled and adjusted to the ship speed. The interceptor system more efficiently controls trim due to pressure at the stern area (17-20). The controllable device helps to adjust the interceptor's height and is suitable to increase the effectiveness of using the interceptor with adjustments to ship speed (21). Therefore, it is necessary to review the ship speed, hull shape, and appropriate interceptor height before installing this device. Shear and pressure resistance are also discussed in the literature (22).

Changes the interceptor design will affect the ship flow patterns and resistance. This research assumed that the bulb interceptor would create an ideal flow pattern on high-speed vessel. Viscous flow that passes through the bulb will cause stagnation, wake, drag, and its relationship with flow separation (23). Experimental research used a small cylinder as a passive controller to reduce drag (24). The research showed an average maximum drag reduction of 48% on a cylinder without a passive controller. Modifying into the bulb interceptor is expected to improve ship flow at high speeds.

This research was observed on the computational fluid dynamic (CFD) based on the finite volume method (FVM). This method was used to solve differential analytical into algebraic equations that could be solved through an iteration process. The CFD method would more easily show and analyze the shape and dimensions of an object, environmental conditions, and interpretation of research results. There was no expense involved in producing ship prototypes using CFD instead of the experimental technique. The results could be more clearly visualized using the CFD technique. CFD may display phenomena including pressure, wave pattern, trim angle, heave, and total resistance that are turned on by the ship's reaction. Using the ITTC's recommendation and compared to experimental results according to specific circumstances.

The problem that occurs with the interceptor is producing excessive trim at high speed. The interceptor is not recommended at high-speed conditions (19). In the condition when the moment of the interceptor was less than the trim moment, the interceptor efficiency would be weak. However, if the moment of the interceptor were more significant than the trim moment, the interceptor would not be feasible to use. On an interceptor with weak efficiency, the ship trim is not well controlled, while on an unfit interceptor, it can cause negative trim while increasing the ship resistance (25). Therefore, we provide interceptor bulb innovation to improve interceptor performance at high speeds. The difference we make with the Keuning patent (26) is that the shape of our interceptor is a half bulb. Our studies are based on several studies that analyze the hydrodynamic characteristics of the shape of objects. The flow separation on the interceptor bulb causes a different wake than the rectangular interceptor. The velocity of flow separation is directly proportional to wake and drag generated by the interceptor. According to an analysis of the proper orthogonal decomposition (POD) mode distributions for the four various angles of attack, the baseline hydrofoil produces flow energy distributions that are significantly different among those surrounding it (27). The size of the riblets significantly influences the impact of drag reduction. The riblets function as a friction-reducing hiding. More than 13% of drag can reduce by holding gases in transverse hydrophobic riblet surfaces. When water flows over a surface, the solid-liquid interface's area and the

boundary layer's velocity gradient can decrease due to slippage at the liquid-gas interface caused by the existence of both gas and vortices in the riblet valley (28).

2. METHOD

2. 1 Research Object Seven hulls are being developed to serve as a platform for an autonomous unmanned surface vehicle (USV). Another research was developed three deep-V hull forms. The resistance and seakeeping performance of the hulls are determined (29). ”Aragon 1” is the name given to the full-scale vessel that employs the fifth hull form. The sixth and seventh hull forms are designed to enhance straight-line stability and maneuverability. The sixth hull form is modified to construct the full-scale vessel ”Aragon 2.” The final hull has been designed based on accumulated experience and is currently being constructed on the full scale. This study uses the scale factor and the size of the interceptor regarding the experimental study carried out (16). CFD simulation testing was carried out using a 1/5.33 scale model. Table 2 shows the interceptor dimensions, consisting of a rectangular interceptor and a bulb interceptor. Figure 1 indicates the hull form of Aragon 2, visualizing the bulb interceptor and rectangular interceptor. The stated figure also explains the location of the interceptor in the stern area and the interceptor size in mm.

2. 2. Research Method This research referred to the ITTC to ensure numerical accuracy (30). To compute flows in the presence of overset mesh, the numerical grid must be customized to the moving body and hence move with it. In order to adjust for grid movement, the governing equations must be given

TABLE 1. Main Dimension of Aragon 2 Ship

Dimension	Full-scale	Model-scale	Unit
Length overall (Loa)	8000	1500	mm
Length waterline (Lwl)	7539	1414	mm
Breadth overall	2300	431	mm
Draft	445	83	mm
Weight	3000	19.77	Kg

TABLE 2. Main Dimension of Interceptor

Dimension	Rectangular interceptor	Bulb interceptor	Unit
Length (L)	300	300	mm
Thickness (T)	20	-	mm
Diameter (D)	-	60	mm
Height (H)	30	30	mm

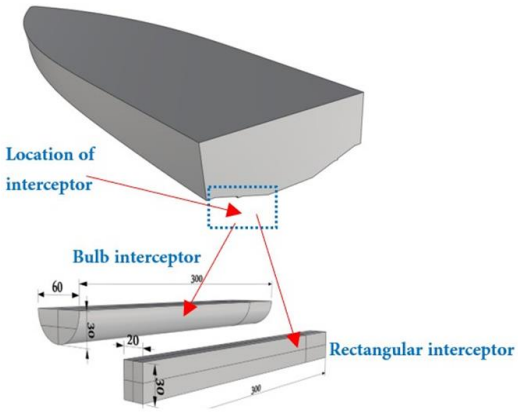

Figure 1. Implementation of Interceptor

special consideration. The overset mesh is to rewrite the Arbitrary Langrangian- Eulerian using CFD software. Mass, momentum and scalar equations are shown at this formula; for V as a control volume, S as a moving surface and V_s is the velocity of the CV-surface.

$$\frac{d}{dt}\int_V \rho\, dV + \oint_S \rho\,(V - V_s)\cdot d_S = 0,$$

$$\frac{d}{d_t}\int_V \rho u_i\, dV + \oint_S \rho u_i (V - Vs).ds =$$

$$\oint_S \mu\, grad\, u_i\, .ds + \int_S \mu\,[(grad\, v)^T.i_i].ds -$$

$$\oint_S p\, i_i.ds + \oint_V \rho\, f_{bi}.dV, \frac{d}{d_t}\int_V \rho\phi\, dV + \oint_S \rho\phi(V -$$

$$Vs).ds = \oint_S \Gamma\phi\, grad\, \phi.d + \int_S Q\phi S.ds + \oint_V Q\phi V.dV,$$

Figure 2 describes the boundary conditions and the computational domain. The inlet, top, and bottom areas were defined as the inlet velocity. Meanwhile, the outlet boundary conditions were defined as pressure outlets. This section has placed some distance from the ship to minimize geometric disturbances. The symmetry plane was used to divide the computational domain into several areas. It was used to reduce computing time. The meshing method used was overset mesh. The overset method have a better accuracy rate than other methods (31, 32). The overset mesh method required at

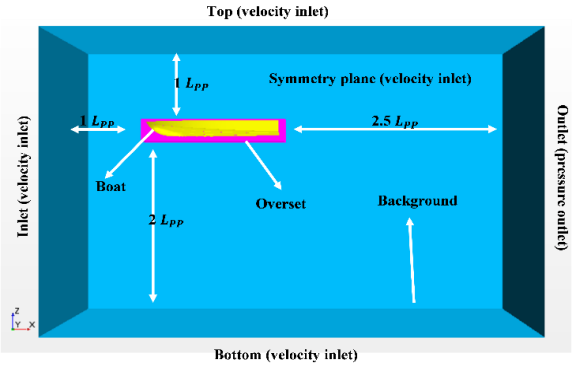

Figure 2. Boundary Conditions

least two different areas as overlapping areas for information exchange. There was a background as a donor and an overset as a donor recipient. The background region provided a visualization of the entire computational domain. Meanwhile, the overset region defined the 2 degrees of freedom of the ship (heave and trim). Acceptor cells receive information from a region through interpolation.

Figure 3 describes the compositions of mesh density. Mesh density variation is vital to reduce computation time. The level of mesh density is focused on the free surface and geometry area. The unstructured mesh was used for flexibility in adapting the mesh to domain boundaries.

The time step in Figure 4 describes the time interval period for each simulation. The time step was determined by the CFL (Courant Friedrichs Lewy) number to explain the number of points traversed by the fluid in a specific time interval. The time step ensures that convergence is achieved in the maximum number of iterations per time step. The VOF method considered the same pressure and velocity for each phase of the control volume. To determine the value of each time step approach (33).

Based on the local cell fluid velocity, the *y*+ value represents the non-dimensional distance from the wall to the first mesh node. Figure 5 represents the thickness of the first layer of mesh and the level of numerical accuracy. Recommendation *y*+ on high-speed craft between 30 and 100 [30].

In this research, the y^+ value ranged from 75. Viscous and inviscid fluids were separated by a boundary known as the boundary layer. The section that was influenced by the viscous effect was that which fell between the solid surface and the boundary layer. The boundary layer, which separates viscous and inviscid fluids, was present. The region that was impacted by the viscous effect was that which became between the solid surface and the boundary layer. Wall shear stress depends on y+ in the process. In order to suggest an iteration scheme, it becomes very computationally costly to perform wall shear stress iteratively for every mesh cell, especially when many boundary cells are involved (34).

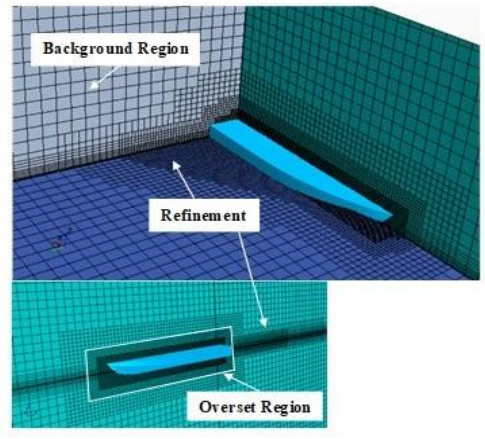

Figure 3. Mesh Density

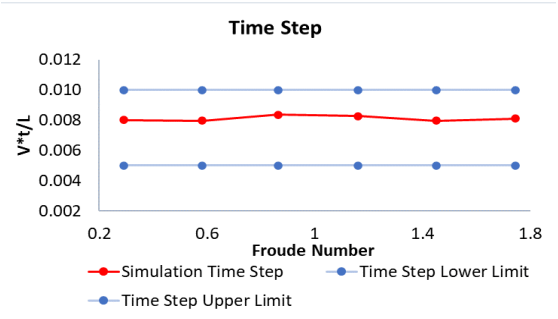

Figure 4. Time Step

3. RESULT AND DISCUSSION

3. 1. Grid Independence Study This research used a grid independence study to determine the best mesh quality. Five grid variations consisted of 0.52, 0.66, 0.87, 1.24, and 1.47 million. Figure 6 visualizes the sample on the grid variation used in this research. Grid-spacing and time-step convergence study were carried out following the correlation factor (CF) and GCI methods of Roache. Grid 4 had better mesh density characteristics than grid 3. The grid analysis consisted of drag, trim, heave, and the time required, as described in Figure 7.

Drag value on each grid as shown in Figure 7a. Furthermore, in Figure 7b, the trim value was generated for each variation of the mesh size. Figure 7c represents the data heave in this grid independence study. After reviewing the time required during data analysis, as described in Figure 6d, it was found that grid five took a relatively long time, so grid four was chosen for each simulation.

The grid four convergence study is detailed in Figure 8, which presents drag, trim, and heave on the Froude number 1.072. This analysis illustrates that the convergence study was stable at second physical time.

3. 2. Validation of the Numerical Method The CFD simulation was verified by experimental research

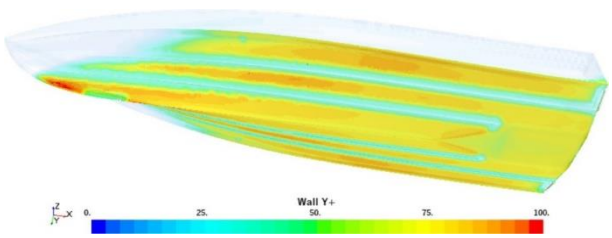

Figure 5. Visualization of Y+

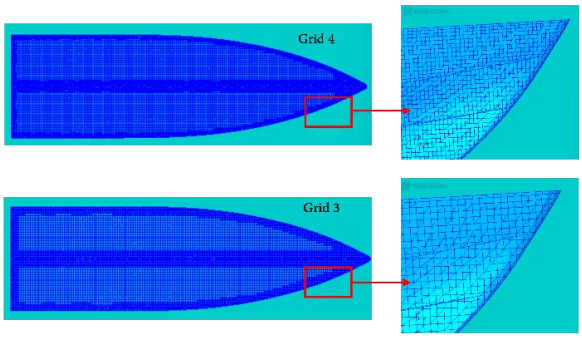

Figure 6. Grid Visualization

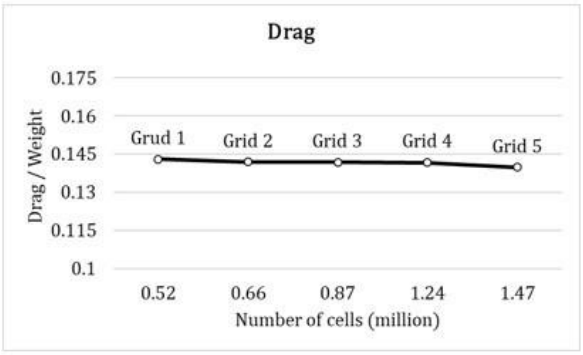

Figure 7a. Drag Value

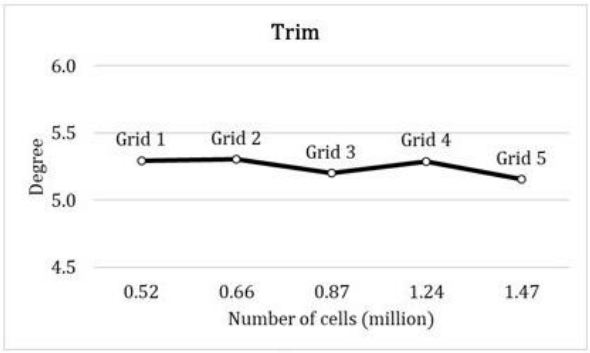

Figure 7b. Trim Value

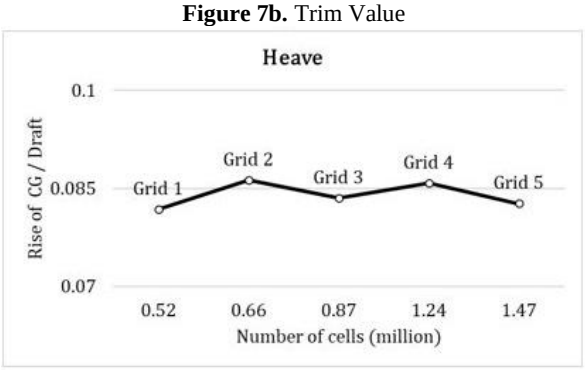

Figure 7c. Heave Value

to ensure reasonable accuracy by reviewing drag, trim, and heave through six variations of the Froude number for bare hull conditions. The CFD simulation shows the same pattern as the experimental results. In Figure 9a,

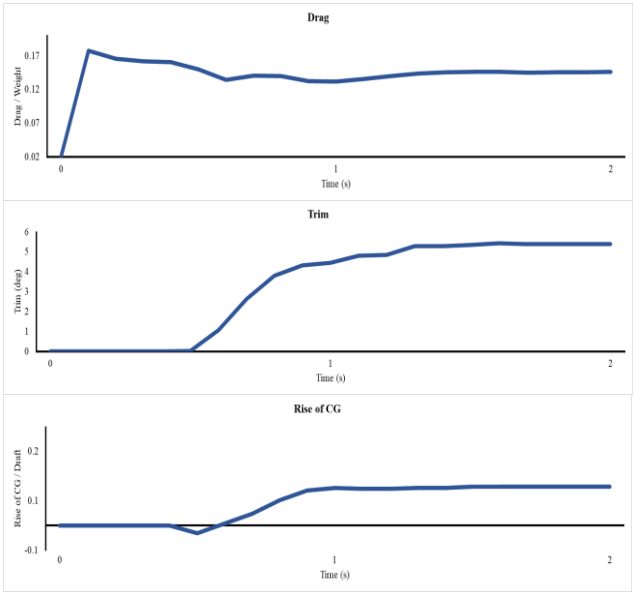

Figure 8. Grid Convergence

the difference in the maximum drag value was 9.9%. Furthermore, the maximum difference in the trim value in Figure 9b was around 10.7%. The heave value in Figure 9c had a maximum error of 10%. There was a difference between CFD calculations and experiments because of the limitations of CFD modelling according to actual conditions. The difference that was still acceptable concerning the CFD method and the same pattern was produced. The same case also occurred in research, which observed the CFD accuracy in experiments and obtained a 10% error (35, 36).

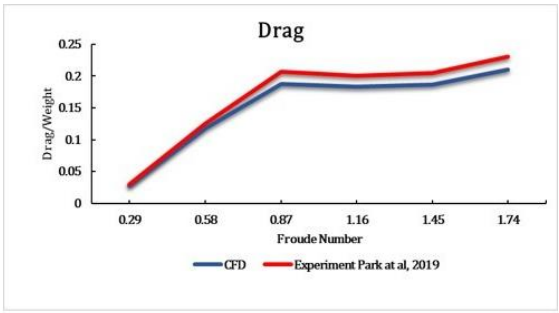

Figure 9a. Drag Value

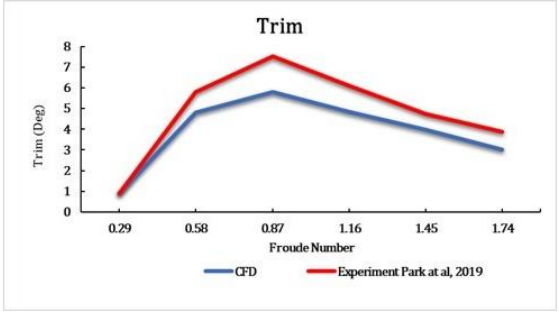

Figure 9b. Trim Value

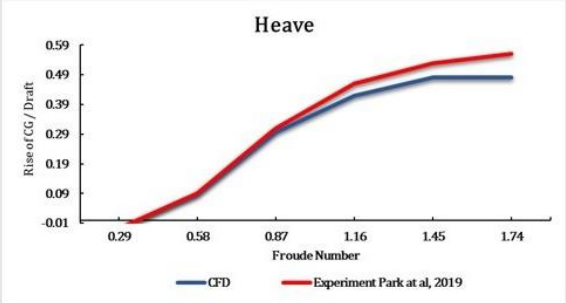

Figure 9b. Heave Value

3. 3. Research Result of Bulb Interceptor Comparing Rectangular Interceptor The pressure distribution is shown in Figure 10. There was a difference in the composition of pressure distribution between ships with bulb interceptors, rectangular interceptors and bare hull conditions. Bare hull conditions showed the centre of the pressure distribution was located near the bottom of the ship at Froude number 1.45. At the same speed, the pressure distribution produced by the bulb interceptor and rectangular interceptor was at the stern position of the ship. The same pattern showed that at a speed of 0.58, the bulb and rectangular interceptors produced a pressure distribution on the stern with a lower value than the Froude number 1.45

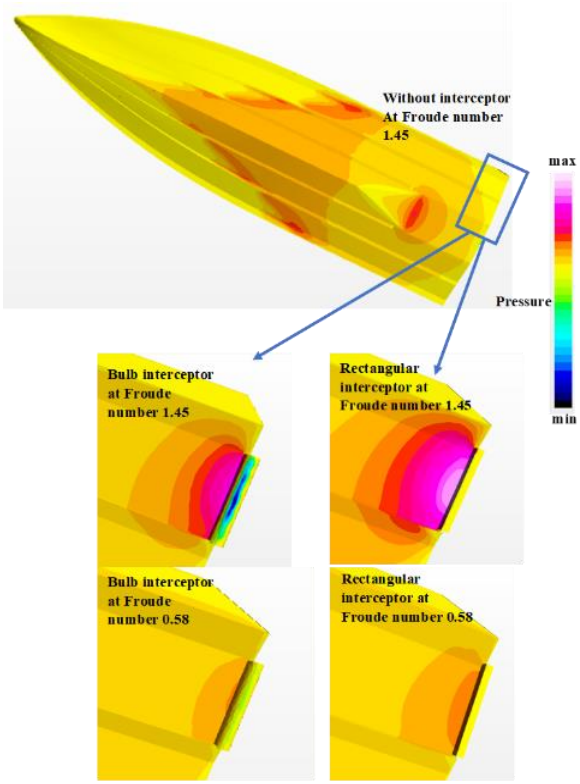

Figure 10. Pressure Distribution

Figure 11 shows the wave elevation on the ship at Froud Number 2.59. The rectangular interceptor produced a relatively high wave elevation in the transom of the ship. Meanwhile, a gentle flow was formed due to the use of a bulb interceptor. The flow produced by the bulb interceptor supported the ship's reasonably good performance at high-speed conditions.

Figure 12 describes the visualization of the air-water multiphase flow by the ship. At Froude number 0.29, both interceptors did not significantly affect the flow pattern at the stern. In Froude number 0.87, there was a significant difference. The rectangular interceptor produced a smaller flow than the bulb interceptor. At Froude number 1.45, the rectangular interceptor produced a trim of 1.84 degrees, while the bulb interceptor produced 2.98 degrees. Froude numbers 2.01 and 2.59 had ineffective trim values of 0.389 and -0.155 degrees.

Meanwhile, at the same Froude number, the bulb interceptor produced the ideal trim of 1.729 and 0.99 degrees. It proved that the bulb interceptor was better applied to the transition and planing phases. However, the vessel had ineffective hydrodynamic forces at the bare hull conditions.

As shown in Figure 13, the viscous flow passing through the bulb interceptor increased pressure on the downstream side. When the momentum of the fluid flow is lower than resist the pressure of the vessel, it will induce the fluid flow separation. The area after the separation point had a smaller pressure than the area on the upstream side, resulting in a significant pressure difference.

The fluid flow velocity would decrease or stagnate in front of the bulb. Along with the fluid flow velocity, the pressure on the stern surface of the downstream ship

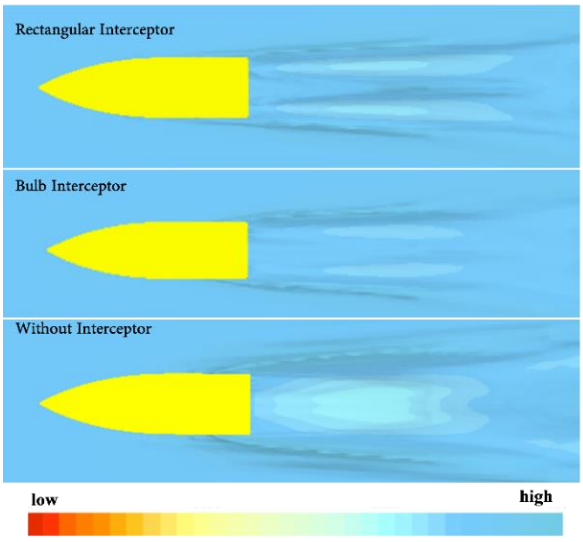

Figure 11. Wave Elevation at Froude Number 2.59

area would be higher. Point a was the stagnation point, and then the boundary layer occurred. From point a to point c, there was a decrease in velocity, which increased pressure. At point C, the flow momentum could not resist the shear stress, causing the boundary layer to break. Between the points of separation of the boundary layer, there was an area called a wake. The amount of wake was directly proportional to the difference in drag force in the downstream and upstream areas of the interceptor bulb.

Figure 14 describes wake diffraction on a ship using rectangular and bulb interceptors in Froude number 2.01. This figure indicated differences in wake contours due to differences in the shape of the interceptor. The stern area is shown in notation 1. Notation 2 described the pneumatic system for adjusting the height of the interceptor. Notation 3 was a visualization of a rectangular interceptor that could produce a wake flow, as described in notation 4. Notation 5 was a visualization of wakes formed without an interceptor installation. Notation 6 was a description of the bulb interceptor. Notation 7 was the wake pattern created by the interceptor bulb. Ships using interceptor bulbs could produce less extreme wakes than ships with rectangular and without interceptors.

The size of the drag force was determined by the period of flow separation. If the separation occurred earlier, the wake region would be more expansive, and the drag would be higher. Factors determining the separation position on the bulb interceptor included: free stream velocity and flow profile, free stream turbulence, geometric shape, and body surface roughness. Figure 15 compares the analysis results of variations in the interceptor's shape to the ship's hydrodynamic characteristics. Generally, a rectangular interceptor was applied in the hump region condition (transition mode). However, a rectangular interceptor was not recommended for full-speed ship conditions because it caused excessive trim and increased ship resistance [25].

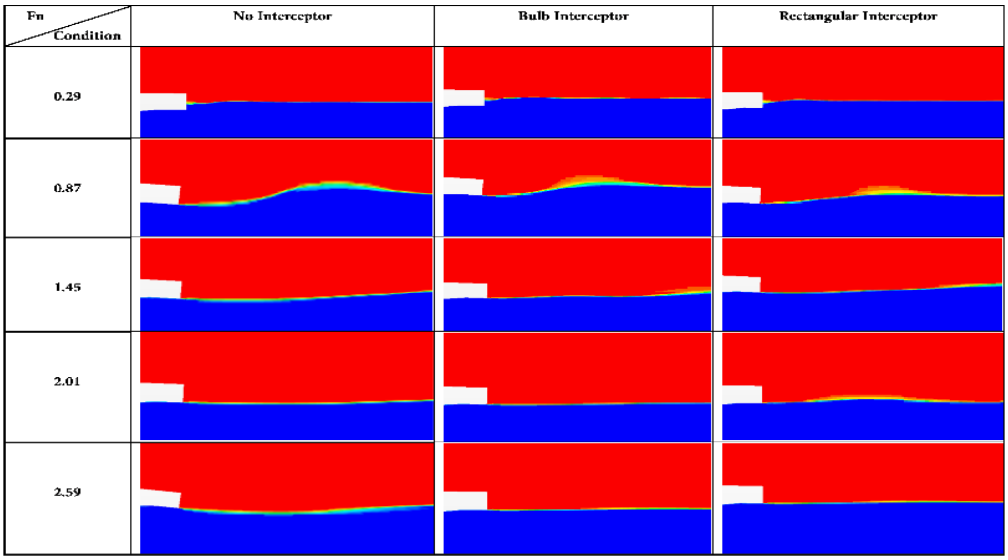

Figure 12. Multiphase Flow Simulation

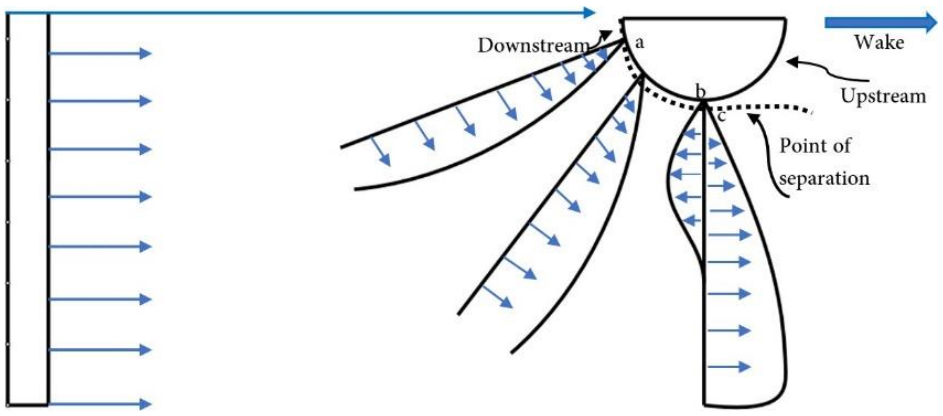

Figure 13. Wake and Point of Separation

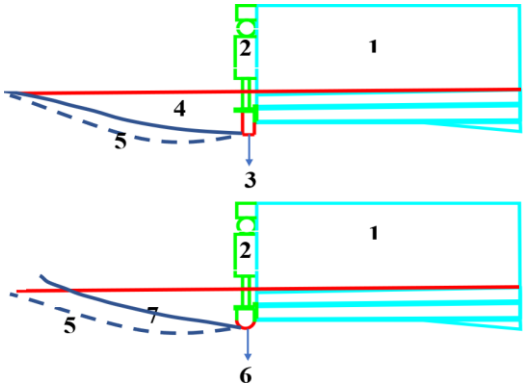

Figure 14. Wake Diffraction at Fn 2.01

The latest phenomenon in this paper describes using a bulb interceptor identical to the rectangular in the hump region condition. However, the complete or full speed condition or more than 1.16 did not worsen the obstacle condition. It was supported by the trim angle, which did not experience negative trim up to Froude number 2.59. One time, accidentally using a bulb interceptor at high speed would not worsen the ship's performance like a rectangular interceptor. On the contrary, it would improve the ship's trim and reduce drag.

Figure 15a represents the ship's drag data. Compared with the rectangular Interceptor, the bulb interceptor was less effective in the pre-planning and transition phases, namely the Froude numbers 0.29, 0.58, and 0.87, with a difference in a drag reduction of 5%, 4%, and 3%. This research illustrated decreased drag components as much as 4%, 24%, and 34% at Froude numbers 0.29, 0.58, and 0.87 in the current bulb interceptor condition compared to without Interceptor. The bulb interceptor had excellent effectiveness compared to the rectangular Interceptor at Froude numbers 1.16, 1.45, 1.74, 2.01, and 2.59, with a drag reduction of 12%, 15%, 29%, 40%, and 49%. If the bulb interceptor were compared with no interceptor at the same speed, it would reduce drag by 3%, 28%, 29%, 20%, and 13%.

Rectangular Interceptor was not recommended for use at high speeds because it would cause an increase in drag of 14% and 24% on Froude numbers 2.01 and 2.59. In this phase, the rectangular Interceptor had a high enough pressure, but the bulb interceptor had sufficient dimensional slope characteristics to reduce excess pressure at high speeds.

Figure 15b visualizes the trim value for each variation of the interceptor and ship in bare hull condition. In general, the trim value in the bulb interceptor condition was more effective than other variations because the ship did not experience bow-down or bow-up trim. The trim condition was reasonably representative of the ship being in a condition close to an even keel and having the best optimization of drag reduction compared to the rectangular interceptor and without an interceptor. The same thing is also shown in Figure 15c regarding the heave value. The heave produced by the bulb interceptor, rectangular interceptor, and without interceptor had the same pattern for the speed range of 0.58 to 2.01. However, using a bulb and a rectangular interceptor could reduce the heave value at the Froude number 2.59.

Using a rectangular interceptor and a bulb at low speeds can provide better performance than without an interceptor. At high speeds, the rectangular interceptor causes an increase in drag and creates excessive trim, making it dangerous for the safety of the ship. If the rectangular interceptor is used at high speed, it can

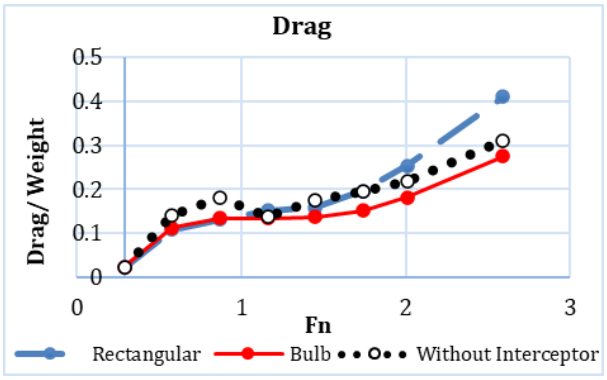

Figure 15a. Drag Value

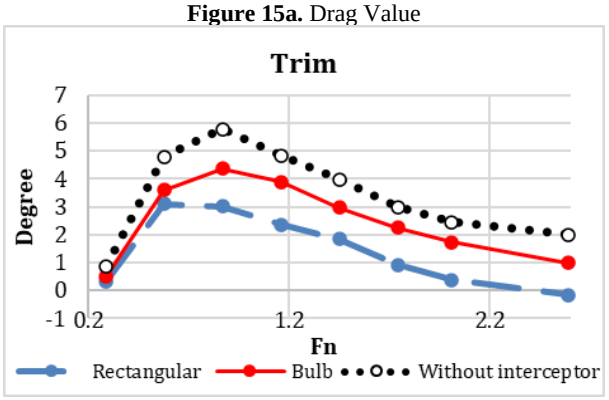

Figure 15b. Trim Value

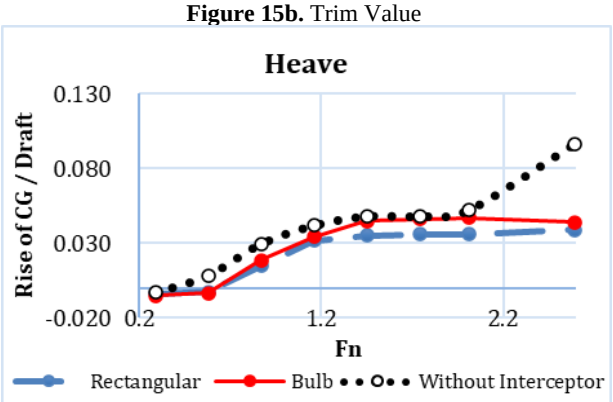

Figure 15c. Heave Value

cause the ship to capsize. Nevertheless, the interceptor bulb can reduce resistance at high speeds and produce an ideal trim for vessel comfort. When the speed is high, the ship's performance due to installing a bulb interceptor is more promising than a rectangular interceptor or without an interceptor. Using interceptor bulbs at high speeds can support ships to reduce drag and prevent capsizing effects.

4. CONCLUSIONS

The main objective of this research was to provide information about interceptor design innovation for an autonomous unmanned surface vehicle. This paper discussed the effect of the different shapes of the interceptor, namely bulb and rectangular, so that it affected trim, drag, and heave.

This research showed the ability of numerical simulation through grid independence study. Five mesh quantity grids were simulated to get the best mesh configuration used throughout the simulation. This study was conducted following the ITTC recommendations. The CFD study was compared with the experimental results. The level of numerical accuracy provided relevant results for the experiment with an error of 10.7%.

Ships without interceptors produced pressure distribution in the centre of the bottom of the ship. In general, the interceptor application had implications for the pressure distribution.

The interceptor changed the centre of the pressure distribution to the stern of the ship's bottom area. The force affected the trim angle of the ship. The rectangular interceptor was usually adequate for Froude numbers 0.58 – 1.16. However, at high speeds, it would worsen the ship's performance.

This research found that the pressure produced by the bulb interceptor was lower than the rectangular interceptor, so the moment created by the interceptor is not excessive. In addition, the bulb interceptor produced a smoother wake pattern behind the ship's stern to support trim improvements. The research results indicated that the interceptor bulb's application positively affected Froude number 1.16. If the interceptor is used at high speed, it will reduce the ship's resistance. At Froude number 1.74, the trim angle of the ship was in the range of 0.99-1.72, so the ship was still optimal to operate. The trim angle represented the best optimization of drag reduction compared to ships using a rectangular interceptor or without an interceptor. Ships using rectangular interceptors would experience bow-down trim at Froude number 2.59.

The viscous flow in the interceptor bulb experienced increased pressure at the downstream position. The pressure difference between the downstream and upstream areas resulted in fluid flow velocity and separation changes. This phenomenon would affect the wake and drag formed on the ship. This research showed that the bulb interceptor had better effectiveness than the rectangular interceptor especially at high-speed condition. The characteristics of the bulb interceptor could manipulate the flow formed at the stern, reducing drag and trim of the ship. According to this investigation, the bulb interceptor surpassed the rectangle interceptor at high speed by 9% to 25%.

5. ACKNOWLEDGMENTS

This research was funded by Ministry of Education, Culture, Research, and Technology of Indonesia, grant number 187-06/UN7.6.1/PP/2022. The authors appreciate the laboratory of ship hydrodynamics Universitas Diponegoro for providing computer resources.

6. AUTHOR CONTRIBUTIONS

Serliana Yulianti: Conceptualization, software, validation, writing original draft; Samuel: Investigation, writing-review, funding acquisition; Parlindungan: Investigation; Syaiful Tambah: Investigation

7. REFERENCES

1. Han J, Cho Y, Kim J, Kim J, Son Ns, Kim SY. Autonomous collision detection and avoidance for ARAGON USV: Development and field tests. Journal of Field Robotics. 2020;37(6):987-1002. https://doi.org/10.1002/rob.21935
2. Perera LP, Ferrari V, Santos FP, Hinostroza MA, Soares CG. Experimental evaluations on ship autonomous navigation and collision avoidance by intelligent guidance. IEEE Journal of Oceanic Engineering. 2014;40(2):374-87. https://doi.org/10.1109/JOE.2014.2304793
3. Tang P, Zhang R, Liu D, Huang L, Liu G, Deng T. Local reactive obstacle avoidance approach for high-speed unmanned surface vehicle. Ocean engineering. 2015;106:128-40. https://doi.org/10.1016/j.oceaneng.2015.06.055
4. Du X-x, Wang H, Hao C-z, Li X-l. Analysis of hydrodynamic characteristics of unmanned underwater vehicle moving close to the sea bottom. Defence Technology. 2014;10(1):76-81. https://doi.org/10.1016/j.dt.2014.01.007
5. Campana EF, Diez M, Liuzzi G, Lucidi S, Pellegrini R, Piccialli V, et al. A multi-objective DIRECT algorithm for ship hull optimization. Computational optimization and applications. 2018;71:53-72. https://doi.org/10.1007/s10589-017-9955-0
6. Diez M, Serani A, Campana E, Stern F, Campana E, editors. CFD-based stochastic optimization of a destroyer hull form for realistic ocean operations. 14th International Conference on Fast Sea Transportation, Nantes, France; 2017.
7. Budiyanto MA, Novri J, editors. Analysis of convergent and divergent-convergent nozzle of waterjet propulsion by ansys

fluent simulation. RINA, Royal Institution of Naval Architects-5th International Conference on Ship and Offshore Technology: Development in Ships Design and Construction, ICSOT 2017; 2017: Royal Institution of Naval Architects.

8. Yaakob O, Shamsuddin S, King KK. Stern flap for resistance reduction of planing hull craft: a case study with a fast crew boat model. Jurnal Teknologi. 2004;41:43-52. https://doi.org/10.11113/jt.v41.689
9. Budiarto U, Samuel S, Wijaya AA, Yulianti S, Kiryanto K, Iqbal M. Stern flap application on planing hulls to improve resistance. International Journal of Engineering, Transactions C: Aspects. 2022;35(12):2313-20. https://doi.org/10.5829/IJE.2022.35.12C.06
10. Yanuar Y, Fatimatuzzahra F, Alief M, Akbar M, Gunawan G, Wibisono IG, editors. The characteristics of variation the angle of attack hydrofoil on winged air induction pipe toward ship drag reduction using numerical method. AIP Conference Proceedings; 2020: AIP Publishing.
11. Suneela J, Krishnankutty P, Subramanian VA. Hydrodynamic performance of planing craft with interceptor-flap hybrid combination. Journal of Ocean Engineering and Marine Energy. 2021;7:421-38. https://doi.org/10.1007/s40722-021-00211-0
12. Samuel S, Yulianti S, Manik P, Trimulyono A, Firdhaus A, Tuswan T, et al. Numerical Research on the Influence of Interceptor Flaps on the Planing Hydrodynamic Performance. NAŠE MORE: znanstveni časopis za more i pomorstvo. 2023;70(4):219-27. https://doi.org/10.17818/NM/2023/4.4
13. Samuel, Trimulyono A, Manik P, Chrismianto D. A numerical study of spray strips analysis on fridsma hull form. Fluids. 2021;6(11):420. https://doi.org/10.3390/fluids6110420
14. Lakatoš M, Sahk T, Andreasson H, Tabri K. The effect of spray rails, chine strips and V-shaped spray interceptors on the performance of low planing high-speed craft in calm water. Applied Ocean Research. 2022;122:103131. https://doi.org/10.1016/j.apor.2022.103131
15. Molchanov B, Lundmark S, Fürth M, Green M. Experimental validation of spray deflectors for high speed craft. Ocean Engineering. 2019;191:106482. https://doi.org/10.1016/j.oceaneng.2019.106482
16. Park J-Y, Choi H, Lee J, Choi H, Woo J, Kim S, et al. An experimental study on vertical motion control of a high-speed planing vessel using a controllable interceptor in waves. Ocean Engineering. 2019;173:841-50. https://doi.org/10.1016/j.oceaneng.2019.01.019
17. Seok W, Park SY, Rhee SH. An experimental study on the stern bottom pressure distribution of a high-speed planing vessel with and without interceptors. International Journal of Naval Architecture and Ocean Engineering. 2020;12:691-8. https://doi.org/10.1016/j.ijnaoe.2020.08.003
18. Deng R, Chen S, Wu T, Luo F, Jiang D, Li Y. Investigation on the influence induced by interceptor on the viscous flow field of deep-Vee vessel. Ocean Engineering. 2020;196:106735. https://doi.org/10.1016/j.oceaneng.2019.106735
19. Samuel S, Mursid O, Yulianti S, Kiryanto K, Iqbal M. Evaluation of interceptor design to reduce drag on planing hull. Brodogradnja: Teorija i praksa brodogradnje i pomorske tehnike. 2022;73(3):93-110. https://doi.org/10.21278/brod73306
20. Jangam S. CFD based prediction on hydrodynamic effects of Interceptor and flap combination on planing hull. Ocean Engineering. 2022;264:112523. https://doi.org/10.1016/j.oceaneng.2022.112523
21. Sahin OS, Kahramanoglu E, Cakici F. Numerical evaluation on the effects of interceptor layout and blade heights for a prismatic planing hull. Applied Ocean Research. 2022;127:103302. https://doi.org/10.1016/j.apor.2022.103302
22. Samuel S, Yulianti S, Manik P, editors. A Study of the Resistance Components of Planing Hull Using Interceptors. IOP Conference Series: Earth and Environmental Science; 2023: IOP Publishing.
23. Chew Y, Pan L, Lee T. Numerical simulation of the effect of a moving wall on separation of flow past a symmetrical aerofoil. Proceedings of the Institution of Mechanical Engineers, Part A: Journal of Power and Energy. 1998;212(1):69-77. https://doi.org/10.1243/0957650981536736
24. Bouak F, Lemay J. Passive control of the aerodynamic forces acting on a circular cylinder. Experimental Thermal and Fluid Science. 1998;16(1-2):112-21. https://doi.org/10.1016/S0894-1777(97)10010-3
25. Mansoori M, Fernandes A. Interceptor and trim tab combination to prevent interceptor's unfit effects. Ocean engineering. 2017;134:140-56. https://doi.org/10.1016/j.oceaneng.2017.02.024
26. Ju K, Krounbi MT. United States Patent to. 1995.
27. Wei Z, Zang B, New T, Cui Y. A proper orthogonal decomposition study on the unsteady flow behaviour of a hydrofoil with leading-edge tubercles. Ocean Engineering. 2016;121:356-68. https://doi.org/10.1016/j.oceaneng.2016.05.043
28. Fu Y, Yuan C, Bai X. Marine drag reduction of shark skin inspired riblet surfaces. Biosurface and Biotribology. 2017;3(1):11-24. https://doi.org/10.1016/j.bsbt.2017.02.001
29. Kim DJ, Kim SY, You YJ, Rhee KP, Kim SH, Kim YG. Design of high-speed planing hulls for the improvement of resistance and seakeeping performance. International Journal of Naval Architecture and Ocean Engineering. 2013;5(1):161-77. https://doi.org/10.2478/ijnaoe-2013-0124
30. ITTC R. procedures and guidelines: practical guidelines for ship CFD applications, 7.5. ITTC: Boulder, CO, USA. 2011.
31. Yulianti S, Samuel S, Nainggolan T, Iqbal M, editors. Meshing generation strategy for prediction of ship resistance using CFD approach. IOP Conference Series: Earth and Environmental Science; 2022: IOP Publishing.
32. De Marco A, Mancini S, Miranda S, Scognamiglio R, Vitiello L. Experimental and numerical hydrodynamic analysis of a stepped planing hull. Applied Ocean Research. 2017;64:135-54. https://doi.org/10.1016/j.apor.2017.02.004
33. Sukas OF, Kinaci OK, Cakici F, Gokce MK. Hydrodynamic assessment of planing hulls using overset grids. Applied Ocean Research. 2017;65:35-46. https://doi.org/10.1016/j.apor.2017.03.015
34. Hosseini A, Tavakoli S, Dashtimanesh A, Sahoo PK, Kõrgesaar M. Performance prediction of a hard-chine planing hull by employing different cfd models. Journal of Marine Science and Engineering. 2021;9(5):481. https://doi.org/10.3390/jmse9050481
35. Brizzolara S, Serra F, editors. Accuracy of CFD codes in the prediction of planing surfaces hydrodynamic characteristics. 2nd International Conference on Marine Research and Transportation; 2007.
36. Avci AG, Barlas B. An experimental investigation of interceptors for a high speed hull. International Journal of Naval Architecture and Ocean Engineering. 2019;11(1):256-73. https://doi.org/10.1016/j.ijnaoe.2018.05.001

Persian Abstract

چکیده

این مطالعه به دستگاه‌های رهگیر برای بهبود ویژگی هیدرودینامیکی وسیله نقلیه سطحی بدون سرنشین مستقل (USV) می‌پردازد. لامپ و رهگیرهای مستطیلی شکل روی بدنه برنامه ریزی شده بودند. این تحقیق با هدف کاهش تاثیر پسا بر روی رهگیرهای مستطیلی در سرعت های بالا انجام شده است. بر اساس این مطالعه، یک رهگیر لامپ تاثیر بهتری نسبت به یک رهگیر مستطیلی داشت. این تحقیق بر اساس روش حجم محدود (FVM) با برهمکنش دینامیک سیال–بدن (DFBI) است که تریم دینامیکی و غرق شدن کشتی را به تصویر می‌کشد. شبیه سازی از یک تکنیک مش overset با دو دامنه به عنوان سلول گیرنده دهنده استفاده کرد. علاوه بر این، محاسبات عددی با استفاده از معادله رینولدز میانگین ناویر–استوکس و مدل k-turbulence جریان آشفته را پیش‌بینی می‌کنند. مطالعات استقلال شبکه و توصیه‌های کنفرانس بین‌المللی مخزن بکسل (ITTC) برای اطمینان از دقت شبیه‌سازی اعمال شده‌اند. این مطالعه گزارش داد که رهگیر لامپ در مقایسه با رهگیر مستطیلی در سرعت بالا بین ۹ تا ۲۵ درصد کارایی دارد. این تحقیق نشان داد که رهگیر لامپ نسبت به رهگیر مستطیلی کارایی بهتری دارد.